Microstructure and Mechanical Property Improvement of Dissimilar Metal Joints for TC4 Ti Alloy to 304 Stainless Steel Using TA2/Q235 Composite Interlayer

Yan Zhang[1] · YiDi Gao[1] · JianPing Zhou[1] · DaQian Sun[2] · HongMei Li[2]

Abstract

In this work, TA2/Q235 was used as an composite interlayer to prevent the formation of these brittle Ti–Fe intermetallics when joining TC4 Ti alloy to 304 stainless steel (SS). The TA2/Q235 composite interlayer was prepared by explosive welding. The laser was focused on the TC4–TA2 interface, which joined the TC4 and TA2 by fusion welding. At TC4–TA2 interface, a weld zone was formed due to the mixing of molten TC4 and TA2. The laser was focused on the Q235–304 SS interface, a weld zone was formed due to the mixing of molten Q235 and 304 SS. Composite interlayer TA/Q235 was used to prevent the formation of Ti–Fe intermetallics during welding and improve microstructure and properties of the SS–Ti alloy joint. The joint fractured at the TA2/Q235 explosive welding interface with the maximum tensile strength of 548 MPa.

Keywords TC4 Ti alloy · 304 Stainless steel · Composite interlayer · Laser welding · Microstructure · Tensile strength

1 Introduction

Recently, the dissimilar titanium (abbreviated as Ti) alloy to stainless steel (abbreviated as SS) has been highly demanded in aerospace and nuclear industries for welded joint [1]. However, the joining between Ti alloy and SS was faced with great difficulty due to poor metallurgical compatibility of Ti alloy and SS [2, 3]. Direct heat fusion welding of Ti alloy and SS can form various intermetallics, such as TiFe and TiFe$_2$, etc. [4]. These brittle Ti–Fe intermetallics make conventional welded joints cracked spontaneously. All these brittle Ti–Fe intermetallics impair the mechanical properties of the SS–Ti alloy joints [5, 6]. Therefore, the traditional fusion welding has not been technically capable of joining Ti alloy with SS due to a metallurgical incompatibility between them [7]. Moreover, Ti alloy and SS have wide differences in their physical properties, especially the mismatch between

their coefficient of thermal expansion with Ti alloy and SS, which leaves large residual stress in the joints after welding [8, 9]. Therefore, the weld was very brittle and easy to crack under residual stress.

The interlayers such as Cu [9], Ag [10], Ni [6], Al [11] and Mg [12] have been employed to restrain the formation of Ti–Fe intermetallics during butt welding. People seek to minimize the mixing of matrix materials to prevent the formation of these brittle phases, yet even low mixing cannot avoid the formation of brittle Ti–Fe intermetallics. As interlayers form intermetallic phases with Ti and Fe, the strength of such welds depends on brittleness of Ti$_x$M$_y$ and Fe$_x$M$_y$ (M-metal of interlayer) in comparison with Ti$_x$Fe$_y$ and of spatial distribution of intermetallics in the joints. By one pass welding, XiaoYan Gu et al. [13] studied pulsed laser welding of SUS 301L SS to TC4 Ti alloy via pure Nb interlayer. The joint was formed with one welding zone and a reaction layer separated by residual unmelted Nb interlayer. The unmelted Nb interlayer served as a diffusion barrier between Ti and Fe to restrain the formation of Ti–Fe intermetallics. The mechanical performance of the joint was determined by the reaction layer at the Nb-SS interface with a tensile strength of 370 MPa. Yet Fe–Nb intermetallics were formed in the reaction layer, which decreased the mechanical property of the joints. Oliveira et al. [14] joined NiTi to Ti alloy based on laser by using a Nb interlayer. The laser

✉ Yan Zhang
  yanzhang4967@163.com

1. School of Mechanical Engineering, Xinjiang University, wulumuqi 830000, China

2. Key Laboratory of Automobile Materials, School of Materials Science and Engineering, Jilin University, Changchun 130022, China

was located at the Ti6Al4V side of the joint, and the Nb intermediate layer was introduced into the base material as the diffusion barrier. An eutectic reaction was responsible for joining at the NiTi-Nb interface. Furthermore, an eutectic mixture was formed between NiTi and Nb. An average tensile stress of 300 MPa. In this way, Ti–Fe intermetallics can be completely prevented in the joint since the unmelted part of an interlayer served as a diffusion barrier between base materials. How to ensure the quality of joint, the prevention of formation of the Ti–Fe intermetallics, as well as the reduction of the other intermetallics, we should solve the problems. However, the appropriate process parameters and the location of the laser beam spot must be selected to control the formation of the reaction layer in joint. Therefore, this process is too cumbersome and not suitable for industrial production.

Moreover, solid-state welding can eliminate the problems in the direct fusion welding because the base metals remain in the solid state during joining and many successful examples have been reported [15–17]. Kundu et al. [15] have studied Ti–6Al–4V and micro-duplex stainless steel was diffusion bonded in vacuum. Effect of bonding temperature and time on the strength properties at room temperature were evaluated. Shear strength of 397.5 MPa along with 6.5% elongation was obtained for the diffusion couple processed at 850 °C for 90 min. Fazel-Najafabadi et al. [16] achieved friction stir welding parameters were adjusted in order to achieve defect-free dissimilar lap joint of CP-Ti to 304 stainless steel. Joint shear strength was measured; a maximum failure load of 73% of that of CP-Ti was achieved. Mousavi and Sartangi [17] have arrived at a suitable parametric window both analytically and experimentally for explosive welding of CP Ti–SS 304. They have concluded that at low loads formation of intermetallics could be totally avoided. However, the service conditions may make particular processes unsuitable. The diffusion process needs a long time to implement in general. Taking high temperature applications for example, brazing cannot be candidate. Furthermore, the required joint geometry can make friction welding and explosive welding difficult to apply [17]. In fact, the tensile strength of Ti alloy/ steel joints obtained by explosive welding was often high. However, this method was not suitable for complex geometry and mass production. In fact, butt welding of Ti alloy to steel was convenient in technology. As a non-contact fusion joining technique with high efficiency and flexibility, laser welding has made great achievements in the joining of hard to weld materials and dissimilar metals. Laser welding is particularly suitable for welding of materials with high thermal diffusivity and electrical conductivity, crack sensitivity, and different melting points [18, 19]. Therefore, laser was selected as the welding heat source of Ti alloy and SS.

Based on the noted analysis, two welding mechanisms (fusion welding and explosive welding) are combined of avoiding melting and liquid mixing of the Ti alloy and SS during welding. On this basis, a new process for two pass laser welding of Ti alloy and SS with TA2/Q235 composite interlayer was proposed in this paper. The TA2/Q235 composite interlayer was prepared by explosive welding of TA2 and Q235. During welding the laser beam was focused on the TC4–TA2 interface and Q235–304 SS interface, respectively. In this way, a joint with two weld zones separated by unmelted TA2/Q235 composite interlayer was acquired and Ti–Fe intermetallics can be completely avoided in two weld zones. In another word, there is no formation of a Ti–Fe intermetallics during welding. The relation between joint microstructures, mechanical properties and fracture modes was discussed in detail.

2 Experimental Procedures

2.1 Base Materials

The base materials used in this experiment were TC4 Ti alloy and 304 stainless steel. Their chemical compositions and physical properties are given in Tables 1, 2 and 3. It can be seen that there are large differences in thermal conductivity and linear expansion coefficient between the two base materials, which would lead to large temperature gradient and thermal stress in the joint during welding process. The base materials were machined into 100 mm × 80 mm × 1 mm plates, and then cleaned with acetone before welding. Before welding, the specimens were mechanically and chemically cleaned. The gap between the edges of Ti alloy and SS was very important to adequate heat transfer and prevent porosity formation. The specimens are clamped each other tightly in order to get the minimum gap formation between the edges.

2.2 Preparation of TA2/Q235 Composite Interlayer

According to the previous analysis, the composite interlayer was prepared by explosive welding. The interlayer materials used in this experiment were TA2 commercially pure titanium and Q235 low carbon steel. Their chemical compositions are given in Tables 4 and 5. Figure 1a, b show the microstructure of TA2 and Q235, respectively. A schematic diagram of the explosive welding procedure is shown in Fig. 2a. It is shown in Fig. 2b that the optical image of the explosive welding interface. It does not present manifest flaws (micro-cracks and pores), and has a distinct wavy interface. The TA2/Q235 composite interlayer was machined into 80 mm × 4 mm × 1 mm plates, and composite interlayer used was 2 mm TA2 + 2 mm Q235 plate. Before welding, the TA2/Q235 composite interlayer is polished by sandpaper with less granularity to remove oxide film, dirt and other impurities. During grinding, the straightness and flatness of

Table 1 Main chemical compositions of 304 stainless steel (at%)

Si	Mn	P	S	Cr	Ni	N	Fe
0.53	1.07	0.04	0.03	18.09	8.01	0.03	Bal

Table 2 Main chemical compositions of TC4 titanium alloy (at%)

Al	V	Fe	C	N	H	O	Ti
6.06	4.03	0.15	0.02	0.02	0.006	0.17	Bal

Table 3 Physical properties of TC4 titanium alloy and 304 stainless steel

Material	Melting point (°C)	Practical tensile strength (MPa)	Specific heat capacity (J kg^{-1} K^{-1})	Thermal conductivity (W m^{-1} K^{-1})	Linear expansion coefficient (10^{-6} K^{-1})
TC4	1650	1100	536	6.4	8.7
304	1454	685	500	16.3	17.2

Table 4 Main chemical compositions of TA2 (at%)

Fe	C	N	H	O	Ti
0.3	0.1	0.05	0.015	0.25	Bal

Table 5 Main chemical compositions of Q235 (at%)

Si	Mn	P	S	N	Fe
0.30	0.55	0.45	0.05	0.03	Bal

Fig. 1 Microstructures of interlayer materials: **a** TA2; **b** Q235
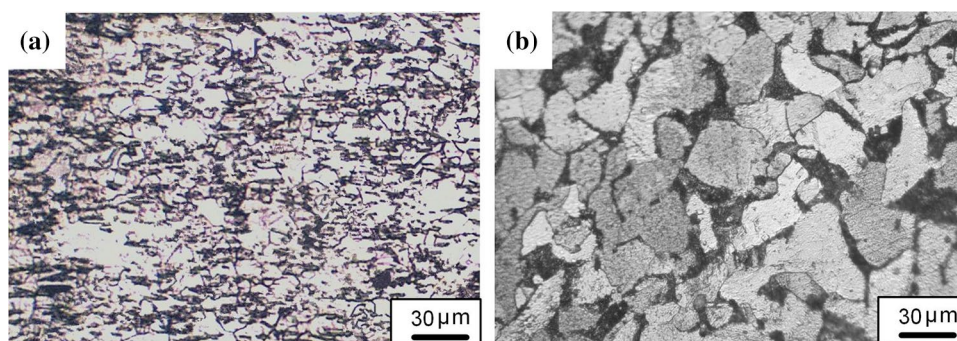
Fig. 2 The making process of composite interlayer: **a** schematic diagram of the welding process; **b** optical image of the explosive welding interface
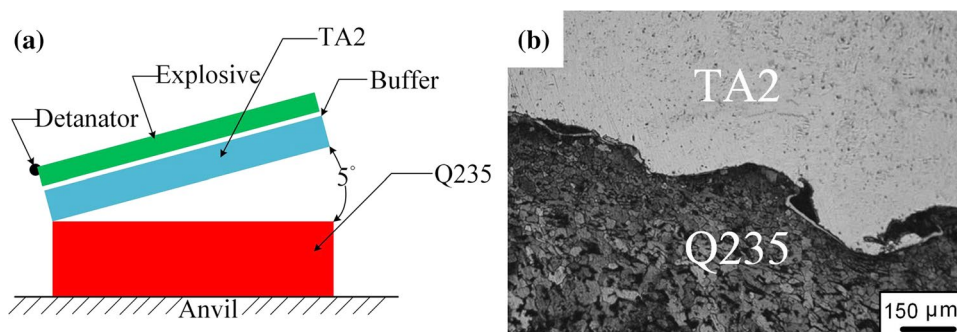

the composite interlayer should be maintained, then ultrasonic cleaning is performed and dried.

2.3 Welding Method

CW laser was used with average power of 1.20 kW, wavelength of 1080 nm and beam spot diameter of 0.1 mm. A schematic diagram of the welding procedure is shown in Fig. 3a. In the first pass, TC4 was welded to TA2 sheet with the laser beam focused on the TC4–TA2 interface, as seen in Fig. 3b. In the second pass (immediately after the first one) Q235 sheet was welded to 304 SS with the laser beam focused on the Q235–304 SS interface, as seen in Fig. 3c. Two pass welding involving creation of a joint with two weld zones separated by remaining unmelted TA2 and Q235. The process parameters of the first pass were as follows: laser beam power of 456 W, defocusing distance of + 5 mm,

Fig. 3 The schematic diagram of the welding process: **a** schematic diagram of the two pass laser; **b** first pass laser; **c** second pass laser
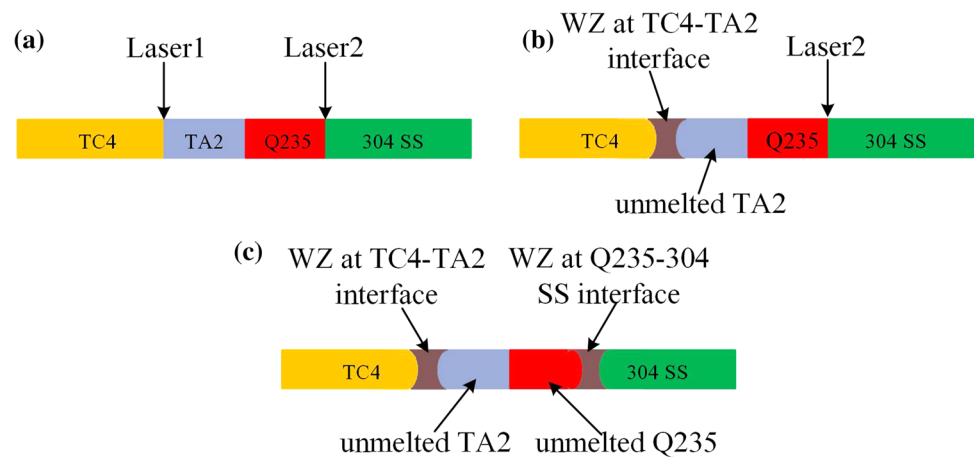
welding speed of 700 mm/min. The process parameters of the second pass were as follows: laser beam power of 492 W, defocusing distance of +5 mm, welding speed of 700 mm/min. Argon gas with the purity of 99.99% was applied as a shielding gas with total flow of 20 L/min at top of the joint.

2.4 Characterization Methods

The cross sections of joints were polished and etched in the reagent with 2 ml concentrated HNO_3 and 6 ml concentrated HF. The microstructure of joints were studied by optical microscopy (Scope Axio ZEISS), scanning electron microscope SEM (S-3400) with fast energy dispersion spectrum EDS analyzer and selected area XRD (X'Pert3 Powder) analysis. Vickers microhardness tests for the weld carried out with a 10 s load time and a 200 g load. Tensile strength of the joints was measured by using universal testing machine (MTS Insight 10 kN) with cross head speed of 2 mm/min. WRN-191K sheathed thermocouple (measuring range −250 to 1350 °C) as the temperature sensor.

3 Results and Discussion

3.1 Macro-characteristics

After welding, the macrostructure of the joint was examined. The cross-section of SS–Ti alloy joint is shown in Fig. 4. As a result, mixing of Ti and Fe was avoided, and brittle intermetallics compounds of Ti and Fe can not be produced. Metallurgical joining was realized through three kinds of metallurgical processes in the joint. The joint can fall into five parts: the first weld zone (WZ_1) formed at the TC4–TA2 interface, unmelted TA2, second weld zone (WZ_2) formed at the TA2–Q235 explosive welding interface, unmelted Q235 and the third weld zone (WZ_3) formed at the Q235–304 SS interface. The WZ_1 did not form Ti–Fe intermetallics due to the presence of unmelted
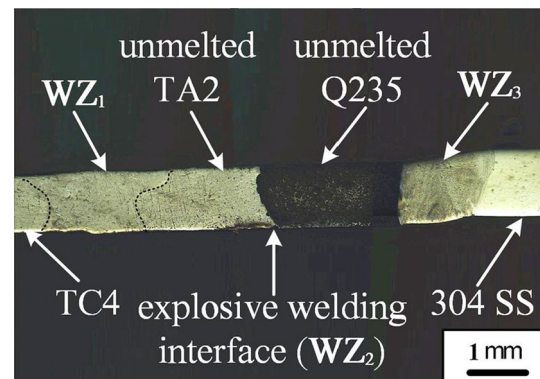
**Fig. 4** The optical image of the cross section of the joint

TA2. Simultaneously, the WZ_3 did not form Ti–Fe intermetallics due to the presence of unmelted Q235. In such a way, a joint with three weld zones separated by the unmelted TA2 and Q235 was acquired, and the formation of Ti–Fe intermetallics can be completely avoided during welding.

It should be noted that precise control of the laser spot position and welding parameters is crucial to obtain a sound joint. If the laser spot is draw near to the TA2/Q235 interface or welding heat input is too large, the TA2/Q235 interface is beginning to melt in the joint, thereby amount of brittle Ti–Fe intermetallics is greatly increased in the joint and cannot be realized the effective combination between SS and Ti alloy.

3.2 Thermal Cycling Test of TA2/Q235 Interface During Two Pass Welding

Based on the noted analysis, TA2/Q235 interface melting must be avoided during two pass laser welding. Therefore, two pass lasers will have a certain impact on the TA2/Q235 interface. To better reflect the formation of the joint, the thermal cycling test was performed on the TA2/Q235 interface.

Fig. 5 Temperature measurement test of TA2/Q235 interface during welding: **a** thermocouple distribution of first pass laser; **b** thermocouple distribution of second pass laser; **b** thermal cycle curve of two test points
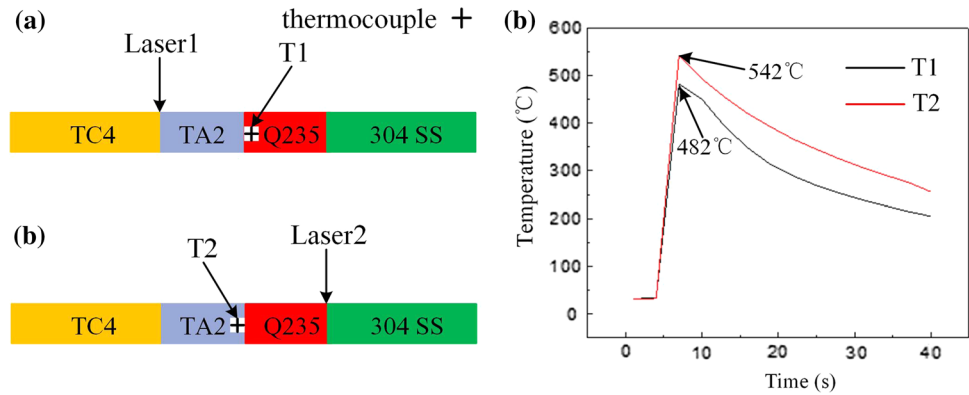
Due to the limitation of plate thickness and clamping device, the welding heat cycle is difficult to test through drilling in the middle or bottom of the test plate. To simplify the test and make the test more precise, this paper studied the heat cycle test from the side slot of the test plate. When the first laser welding, the structure was provided with opposite grooves on the Q235 side faces, and the interior of a sealing groove formed by the groove was provided with a thermocouple, as seen in Fig. 5a. When the second laser welding, the structure was provided with opposite grooves on the TA2 side faces,

structure. The compositions of position A in WZ_1 were studied using SEM-EDS. EDS analysis was applied to each zone in joint to measure the compositions of the reaction products and the results are listed in Table 6. Generally, Mo equivalents are usually used to evaluate the effect of β stable element on microstructure, and several scholars researched the influence of Mo on the phase composition of titanium and found the existence of martensite α′ when $[Mo]_{eq}$ is greater than some values [20, 21].

According to the computational formula [22]:

$$[Mo]_{eq} = [Mo] + 0.2[Ta] + 0.28[Nb] + 0.4[W] + 0.67[V] + 1.25[Cr] + 1.25[Ni] + 1.7[Mn] + 1.7[Co] + 2.5[Fe] \quad (1)$$

as seen in Fig. 5b. The thermal cycle curve obtained from TA2/Q235 interface during welding is shown in Fig. 5c. It is suggested that the peak temperatures of TA2/Q235 interface (first laser welding and second laser welding) were 482 °C and 542 °C, respectively. By the experiment data we can see the the peak temperature of the TA2/Q235 explosive welding interface during the second welding was significantly higher than that of the first welding. This is mainly because the thermal conductivity of Q235 was significantly higher than that of TA2, and the heat input of the second welding was slightly higher than that of the first welding. According to the thermal cycling test of TA2/Q235 interface, the TA2/Q235 interface is at a relatively high temperature during both welding. Through the heat conduction of unmelted TA2 and Q235, two laser welding was equivalent to two post-welding heat treatment of TA2/Q235 interface. This is helpful to reduce or eliminate the residual welding stress of the TA2/Q235 interface due to explosive welding, and improve the strength of composite interlayer.

3.3 Microstructure Analysis

3.3.1 Microstructure Analysis of WZ₁

The optical image of the WZ_1 is shown in Fig. 6a, b, and no defects were observed in it. SEM image of the fusion weld is shown in Fig. 6c. The WZ_1 mainly consists of acicular

According to the computational formula [23]:

$$C_W = D_A C_A + D_B C_B \quad (2)$$

where C_W was the average mass fraction (%) of an alloying element in weld zone; D_A and D_B are the fusion ratios of the two materials in the weld; C_A and C_B are the mass fraction of an alloying element in the materials (%). According to calculation, the fusion ratio of TC4 and TA2 in WZ_1 was 53:47. According to computational formula (2), the average mass fraction of the main elements in WZ_1 can be obtained. According to computational formula (1), the Mo equivalent (Mo_{eq}) of WZ_1 was 3.4. MA et al. [24] found martensite α′ phase in the weld of laser welded homogeneous TC4 Ti alloy (Mo equivalent of weld was 3). Therefore, the main microstructures of WZ_1 were martensite α′. XRD analysis result also confirmed the presence of martensite α′ in WZ_1 (Fig. 6d). A large amount of α′ martensite was formed in the WZ_1 due to the laser welding has faster heating and cooling rate. The α-to-β phase transition and the β-to-α′ phase transition occurred in the WZ_1, resulting in the disappearance of the original α and β phases and the occurrence of a large amount of martensite α′.

3.3.2 Microstructure Analysis of WZ₂

The optical image of the WZ_2 is shown in Fig. 7a. It does not present manifest flaws (micro-cracks and pores). Figure 7b
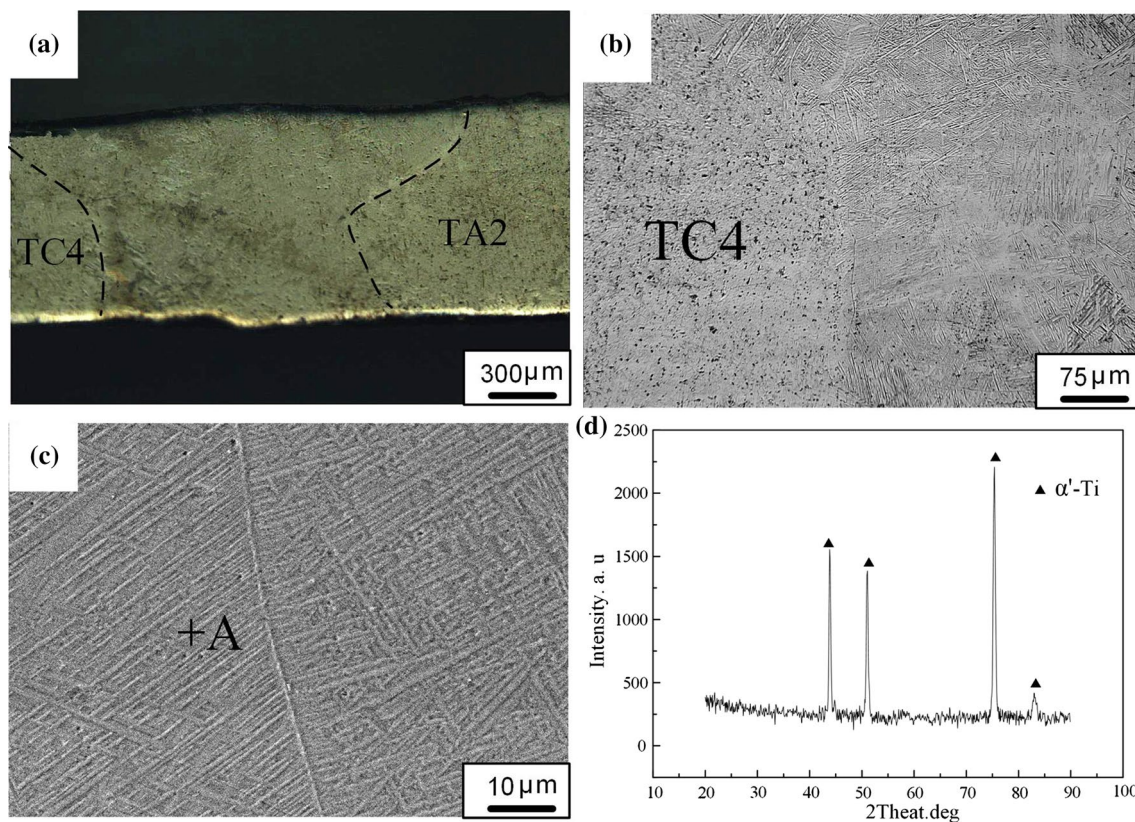
Fig. 6 Microstructures in the WZ_1 of the joint: **a** optical image of WZ_1; **b** optical image of fusion line in WZ_1; **c** SEM image of WZ_1; **d** XRD analysis results of WZ_1

Table 6 The chemical composition of each phase (at%)

Region	Composition (%)							Potential phases
	Ti	Fe	Al	V	Ni	Cr	Bal	
A	97.7		2.3					α′ Martensite
B	67.3	32.7						β-Ti + TiFe
C	83.7	16.3						β-Ti solid solution
D		87.5			3.8	8.7		γ-Fe, α-Fe

exhibits SEM images in different areas of the WZ_2 in Fig. 7a. It can be seen that the WZ_2 consisted of a lamellar structure (marked as B and C). In order to identify the phase structures pointed by arrows in Fig. 3a, the EDS analysis was carried out, as shown in Table 6. Based on the EDS analysis results in Table 6 and Ti–Fe phase diagram [24], zone B was defined as β-Ti + TiFe eutectic and zone C was defined as β-Ti solid solution. The width of zone B and C was 6.3 μm and 4.9 μm, respectively. Thus, finer size dendritic structures were obtained in zone B, which would contribute to minimum brittlement of the WZ_2 [26]. As the Ti–Fe binary phase diagram suggests [25], the maximum solubility of Fe atom in β-Ti atom was 18 at%. Also the single-phase supersaturated β-Ti structure might contribute to fracture resistance because the Fe was a β stabiliser of β-Ti solid solution and broadened

the β-Ti phase zone. Therefore, the main microstructures of WZ_2 were β-Ti solid solution and a small amount of TiFe phase. According to the study by Mousavi et al. [27], TiFe phase has the largest brittleness in the Ti–Fe series compounds. However, the TiFe phase in the WZ_2 presented as a eutectic mixture rather than a single compound layer. It was primarily because the presence of β-Ti solid solution in eutectic structure that reduced the brittleness of TiFe phase. The strength of eutectic structure tended to be stronger than that of single compounds layer. Eutectic structure reduced the brittleness of the WZ_2 due to the presence of β-Ti solid solution. Therefore, it can relatively deform easily to reduce the residual stresses in the inner of joint.

Figure 8 present the SEM-EDS plane analysis results from WZ_2. It can be seen from Fig. 8 that the content of Ti

Fig. 7 Microstructures in the WZ$_2$ of the joint: **a** optical image of WZ$_2$; **b** SEM image of WZ$_2$
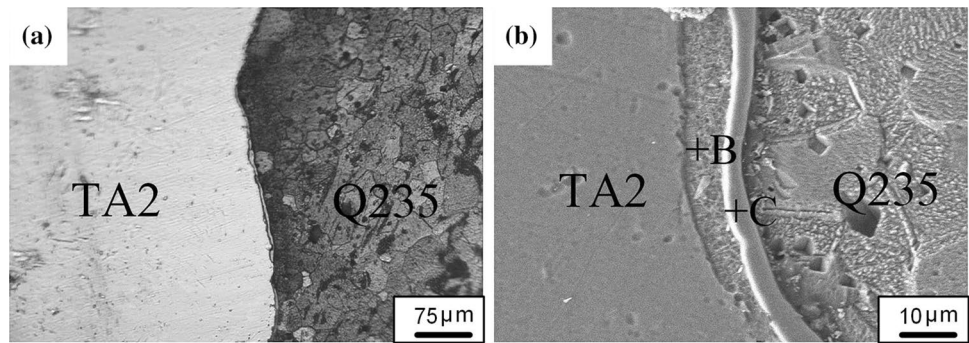

Fig. 8 EDS plane analysis results in the WZ$_2$ of the joint: **a** Ti; **b** Fe
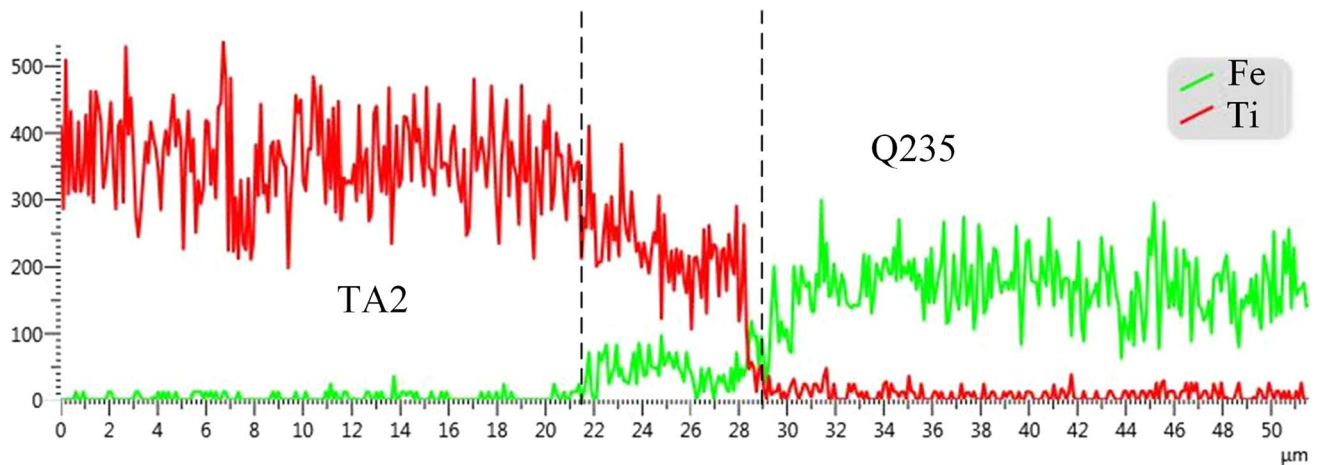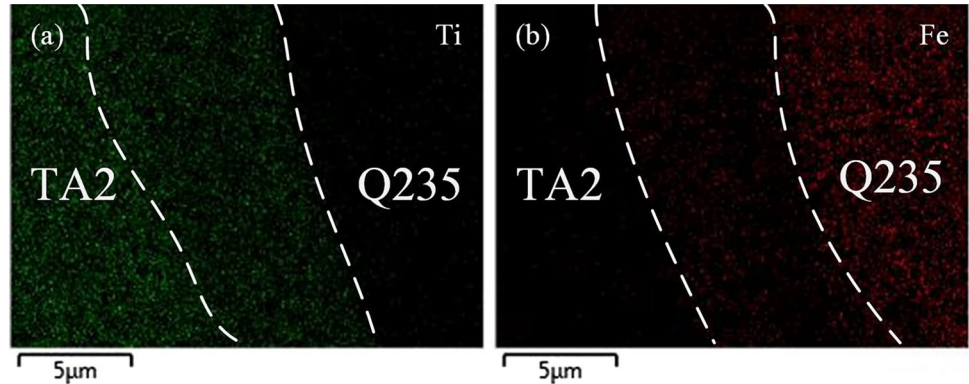
Fig. 9 EDS line analysis results in the WZ$_2$ of the joint

element in the WZ$_2$ is significantly higher than that of Fe element. In order to confirm the elements Fe and Ti distribution in the WZ$_2$, the SEM-EDS line analysis were carried out, as shown in Fig. 9. The line analysis started from TA2 side, passed through the WZ$_2$ and ended in Q235 side. Based on the EDS line analysis in Fig. 9, Fe and Ti, as two main elements, were detected in the WZ$_2$. Moreover, from the TA2 to the Q235, the content of Fe element increased gradually while the content of Ti decreases rapidly as a whole.

The composition abruptly changes at the Q235 side while the transition was more gradual on the TA2 side of the TA2/Q235 interface. This is due to the higher diffusivity of Fe into Ti than Ti into Fe [28]. When Fe diffuse into the TA2 side of the WZ$_2$, the will be dissolved into Ti to form a solid solution. This reaction layer adjacent to the TA2 has a gradual variation in Fe content, and faster diffusion of Fe creates a large amount of vacancies in its matrix, and thus promotes larger diffusional distance of Ti in the Q235 side
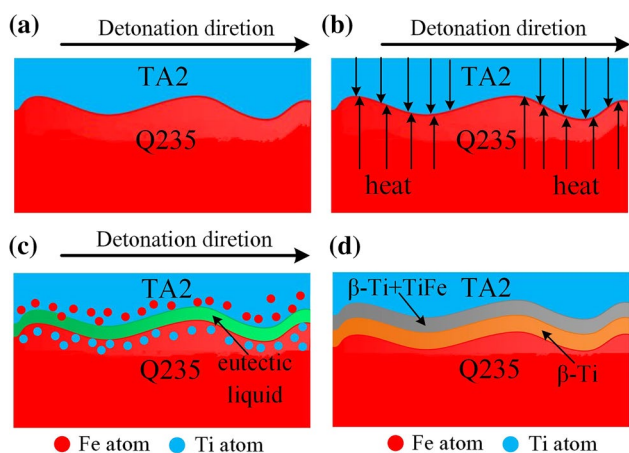
Fig. 10 Physical model formation of the TA2/Q235 interface during explosion welding (**a**) after the ignition of the explosion; (**b**) two surfaces that are in contact with each other to collide at high speed; (**c**) formation of eutectic liquid in the interface; (**d**) formation of β-Ti solid solution zone in the interface

[29]. Fe also penetrates on to the TA2 side inside the alloy composition.

As mentioned earlier, the TA2/Q235 composite interlayer was prepared by explosive welding. The formation model of explosive welding interface (WZ$_2$) is established based on the theory of explosion welding, as shown in Fig. 10. After the ignition of the explosion the TA2 cladding plate accelerates towards the base Q235 plate. A propagating jet forms between the two plates, as shown in Fig. 10a. The flyer plate (TA2 in this case) always undergoes higher deformation than the base material (Q235 in this case) [30]. It uses the impact force generated by explosive blasting to cause two surfaces that are in contact with each other to collide at high speed, thereby converting kinetic energy into heat energy, as shown in Fig. 10b. At higher temperatures, the thermal energy supplied to the diffusing atoms allowed the atoms to overcome the activation energy barrier and to move to new lattice sites more easily [31]. The interdiffusion of Ti and Fe elements occurred until eutectic composition was obtained, and liquid phase was formed through the eutectic reaction, as shown in Fig. 10c. Based on the EDS analysis results in Table 6 and Ti–Fe phase diagram[25], eutectic reaction L → β-Ti + TiFe occurred, and liquid phase was produced at TA2/Q235 interface. The dissolution of Ti and Fe into the eutectic liquid phase occurred under the high concentration gradient. Thus, the liquid phase generation and the element diffusion happened simultaneously. When the temperature was dropped, the β-Ti solid solution zone occurred near eutectic reaction zone, as shown in Fig. 10d. According to the knowledge of metallic physics, the wider the thickness of the reaction zone, the bigger the concentration gradient of Fe in the reaction zone [30]. Therefore, the transform from β-Ti solid solution to β-Ti + TiFe eutectic

structure can be realised easily if there are enough Fe atoms in the β-Ti solid solution/eutectic structure interface, and the eutectic structure zone near the β-Ti solid solution was easier to reach saturation. Subsequently, the Fe and Ti near Q235 side because of high Ti content was not easy to form eutectic structure, which was propitious to the formation of β-Ti solid solution in Q235 side. The conclusion is drawn that the rate of Ti and Fe atoms diffusion was the critical factor to control the formation of WZ$_2$.

3.3.3 Thermodynamic Analysis of Reaction Layer in WZ$_2$

A governing equation was established by Isaac et al. [32] for the widening of the eutectic reaction zone, which reflects the relationship between the thickness of the eutectic reaction zone and the holding time in transient liquid phase. The thickness of eutectic reaction zone was expressed in Eq. (3):

$$W = K(D_L t)^{1/2} \tag{3}$$

W denotes the thickness of the eutectic liquid zone; D_L is diffusion rate of the diffusion element in the eutectic liquid; K is constant; t is the holding time. Since D_L and K are constants at a given temperature. It is suggested that at a constant joining temperature, the thickness of eutectic liquid has linear relation with $t^{1/2}$. The thickness of the eutectic liquid zone can be kept low by shortening the holding time. Because of the explosion welding has a faster heating and cooling rate, the holding time at high temperature was very short, and the liquid phase existed only in a smaller region of the explosion welding (TA2–Q235) interface, which readily forms a narrower eutectic reaction zone (zone B) at the explosion welding interface.

As the analysis suggests, Ti and Fe dissolution and diffusion stage played a decisive role in the growth process of the reaction layer in WZ$_2$. In the welding, the growth of the reaction layer was controlled by the diffusion of Ti and Fe atoms, in which the thickness of intermetallic layer is written in Eq. (4) :

$$X = K_0 \exp(-Q/RT)\sqrt{t} \tag{4}$$

In Eq. (4), X denotes the thickness of intermetallic layer, t is reaction time, n is time factor (0.5), K_0 is constant, R is the gas constant (R = 8.314 J/(mol·K)), Q is the diffusion activation energy and T is the reaction temperature. Equation (4) suggests that both t and T can widen the intermetallic layer, and the contribution from T is considerably larger than that from t. Therefore, the thickness of Ti–Fe intermetallic layer increases with the increase of the reaction temperature at TA2–Q235 interface. As these results suggest, formation and growth of

the coarse Ti–Fe intermetallics at TA2–Q235 interface can be constricted if the heat input in the welding process was small enough. As mentioned before, the explosion welding has a faster heating and cooling rate, the holding time at high temperature was very short. By reasonably controlling explosive welding parameters, the thickness of the Ti–Fe intermetallic layer can be kept comparatively low to obtain a small amount of Ti–Fe intermetallics, which contributes to the mechanical properties of the TA2/Q235 composite interlayer.

3.3.4 Growth Kinetics Analysis of Reaction Layer in WZ_2

As the previous analysis suggests, the main composition phase of the WZ_2 was primarily the β-Ti solid solution and reaction product of Ti and Fe. According to the Ti–Fe binary phase diagram [24], β-Ti, TiFe and $TiFe_2$ compounds can be formed between Ti and Fe. Yet only single β-Ti phase layer was detected in the WZ_2 under the explosive welding. The analysis suggests that the formation of each intermetallic compound was determined first by thermodynamic factors. By conducting thermodynamic analysis, the possibility of the formation of Ti–Fe intermetallics was studied. It is known from the classical physicochemical theory that the free energy of the growing gibbs free energy ΔG is a relative quantity, and the free energy of each substance can be evaluated by the standard free energy:

$$\Delta G_T^\Theta = \Delta H_T^\Theta - T\Delta S_T \tag{5}$$

where T denotes the reaction temperature; ΔG_T^Θ is the standard reaction Gibbs free energy at temperature T; ΔH_T^Θ is the reaction enthalpy change at temperature T; ΔS_T is the reaction entropy change at temperature T. It is the numerical value that can be found in the thermodynamic manual. By calculating the standard Gibbs free energy (G) of the reaction, G can determine whether reaction can proceed spontaneously under constant temperature and constant pressure. When $\Delta G_T^\Theta \geq 0$, the reaction cannot occur spontaneously; When $\Delta G_T^\Theta < 0$, the reaction is spontaneous.

In line with the thermodynamic data of Ti–Fe binary compounds [33], the standard Gibbs free energy G of Ti–Fe intermetallics in the range of 400–1600 °C was calculated, as shown in Fig. 11. It is observed from the diagram that β-Ti, TiFe and $TiFe_2$ reaction free energy can reach − 100 kJ/mol, more than 1000 °C. It is suggested that this reaction was very large in the driving force. During the cooling process, all three are very easy to generate. In particular, the Gibbs free energy of β-Ti phase can reach − 500 kJ/mol, which can be generated at extremely low degree of supercooling. It is observed from Fig. 11 that the Gibbs free energy of β-Ti was much higher than that of TiFe and $TiFe_2$ at the same temperature, so β-Ti will be preferentially generated in the cooling crystallization process.
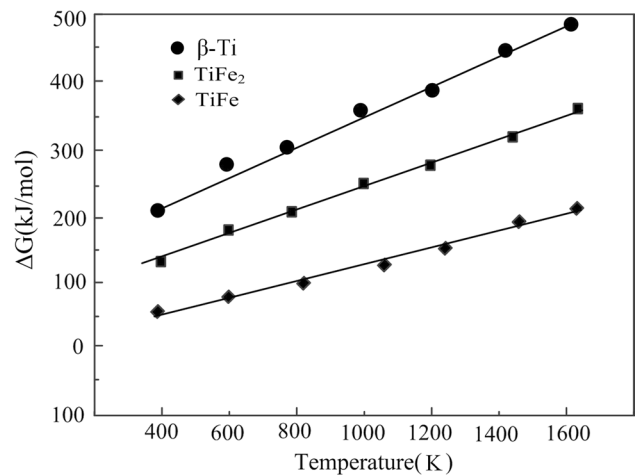

Fig. 11 Temperature varying Gibbs free energy of β-Ti, TiFe and $TiFe_2$

3.3.5 Microstructure Analysis of WZ_3

It is shown in Fig. 12a, b that the optical image of the WZ_3. It does not present such defects as pores and macro-cracks. It is shown in Fig. 12c that the SEM image of the WZ_3. It can be seen in Fig. 12 that WZ_3 mainly consists of columnar crystal. According to calculation, the fusion ratio of Q235 and 304 SS in WZ_3 was 45:55. According to computational formula (2), the average mass fraction of the main elements in WZ_3 can be obtained.

According to the computational formula [34]:

$$[Cr]_{eq} = \%C + \%Mo + (1.5 \times \%Si) + (0.5 \times \%Nb) \tag{6}$$

$$[Ni]_{eq} = \%Ni + (30 \times \%C) + (30\%N) + (0.5 \times \%Mn) \tag{7}$$

According to computational formula (6) and (7), the Cr equivalent (Cr_{eq}) and Ni equivalent (Ni_{eq}) of the WZ_3 were 21.15 and 12.55 respectively, with Cr_{eq}/Ni_{eq} of WZ_3 was 1.69. Based on the carbon equivalence method and Calderon organization chart [35], the main microstructures of the WZ_3 were γ-Fe austenite and a small amount of α-Fe ferrite, the ferrite content in the WZ_3 was approximately 10%. XRD analysis result also confirmed the presence of γ-Fe austenite and α-Fe in WZ_3 (Fig. 12d).

3.4 Microhardness Tests

As shown in Fig. 13, the microhardness distribution in the joint was non-uniform. TC4 Ti alloy has similar hardness to 304 SS. The average microhardness in WZ_1 was 412 HV and was 135% of initial Ti alloy. That could be attributed to the presence of brittle martensite α′ which could make the WZ_1 obtain higher hardness. The average microhardness in unmelted TA2 was 313 HV. The average microhardness in unmelted Q235 was 349 HV. The hardness of TA2 was
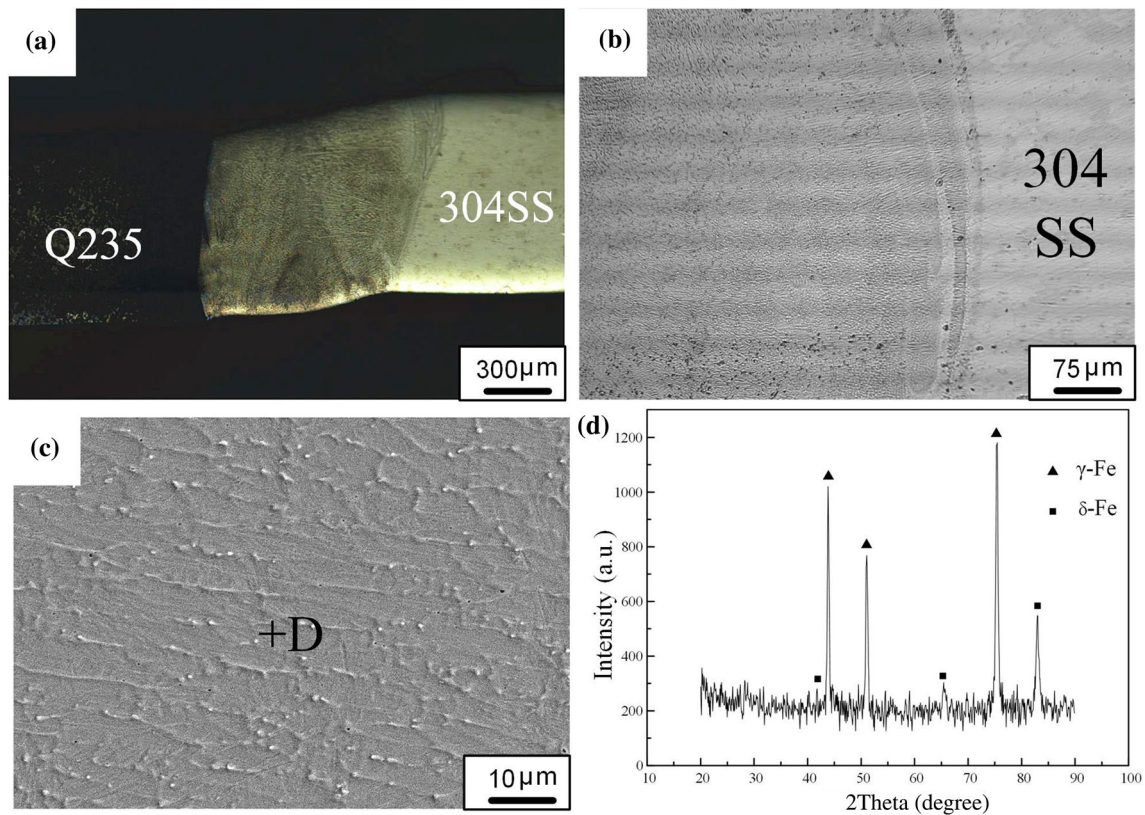
Fig. 12 Microstructures in the WZ_3 of the joint: **a** optical image of WZ_3; **b** optical image of fusion line in WZ_3; **c** SEM image of WZ_3; **d** XRD analysis results of WZ_3
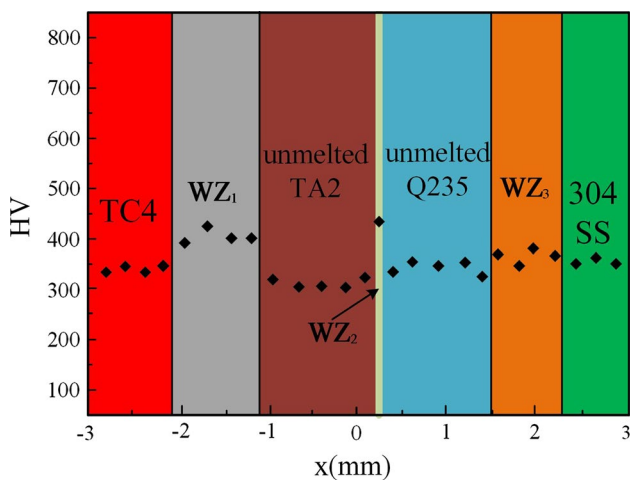

Fig. 13 Vickers microhardness measurements at semi-height of the joint (zero point situated in the center of the joint)

slightly lower than those of Q235. The microhardness in WZ_2 was 422 HV and was 135% of TA2. That could be attributed to the presence of some Ti–Fe intermetallics which could make the WZ_2 obtain higher hardness. The average microhardness in WZ_3 was 343 HV, close to the 304 SS.

3.5 Tensile Tests and Fracture Analysis

As shown in Fig. 14a, the tensile strength of the SS–Ti alloy joint can reach to 548 MPa. To find the weakest part of the joint, the fracture location was analyzed as shown in Fig. 14b. The joint fractured in WZ_2 of the TA2–Q235 interface during tensile tests. Moreover, as shown in Fig. 14c, brittle fracture can be observed at TA2–Q235 interface. The XRD analyses of fracture surface as shown in Fig. 14d. It has also indicated the presence of β-Ti and TiFe phases at fracture surfaces. The WZ_2 of the TA2–Q235 interface became the weak zone of the joint, which led to the failure in the tensile test.

Based on the previous analysis, the TA2/Q235 composite interlayer prepared by explosion welding can control the Ti–Fe intermetallics in a very narrow region to reduce the content of the Ti–Fe intermetallics in the WZ_2. The brittleness of eutectic structure to be lower than that of single Ti–Fe intermetallic layer. The formation of a narrower eutectic reaction zone and the finer size of the eutectic structure and Ti–Fe intermetallics at TA2–Q235 interface were the major reasons for the increase of joint strength. By using explosion welding method, the thickness and size of Ti–Fe intermetallics at TA2–Q235 interface can be controlled,
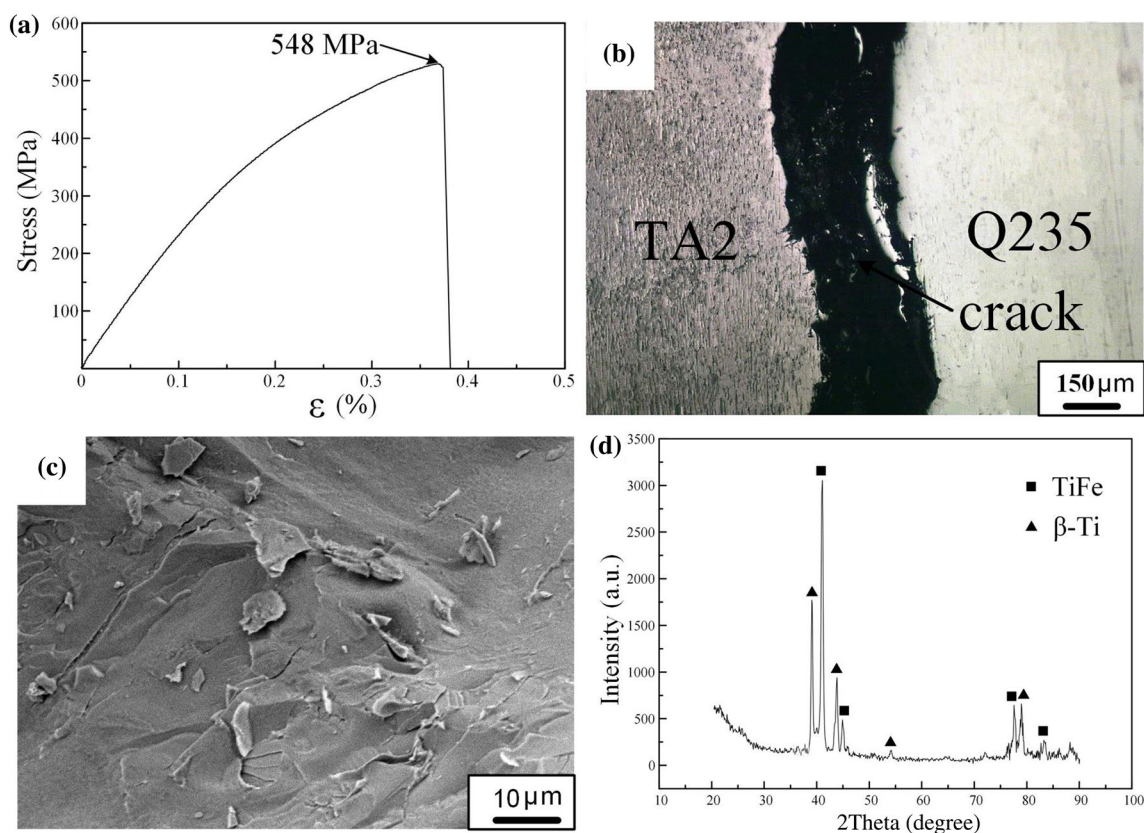
Fig. 14 Tensile test results of the joint: **a** tensile test curve; **b** fracture location; **c** SEM image of fracture surface; **d** XRD analysis results of fracture surface

and the mechanical property of the joint can be improved. Moreover, liquid-state mixing of base metals in SS–Ti alloy joint was avoided by two pass laser welding in this study. Based on above analysis on the joint, it can be concluded that the weld zone at TA2–Q235 interface becomes the weak zone of the joint. The weld zone at TC4–TA2 interface and weld zone at Q235–304 SS interface has a higher strength than the weld zone interface at TA2–Q235 interface. It can be assumed that mechanical property of SS–Ti alloy joint could be improved by improving the strength of the composite interlayer if the composite interlayer is not completely melted during welding.

4 Conclusions

Dissimilar laser welding of Ti alloy to SS was achieved using a TA2/Q235 composite interlayer. The TA2/Q235 composite interlayer was prepared by explosive welding. The nucleation and growth of compounds in the TA2/Q235 explosive welding interface primarily depended on the diffusion rate of Ti and Fe atoms. The Ti–Fe intermetallics produced in TA2/

Q235 explosive welding interface were controlled in a very small region. During welding, the unmelted TA2 and Q235 was selected as a barrier to avoid mixing of the Ti alloy and SS, while ensuring joining at both interfaces (TC4–TA2 and Q235–304 SS). For TC4/TA2/Q235/304 SS joint, all intermetallics formed by Ti or Fe have been avoided during welding. The maximum tensile strength of joint can reach to 548 MPa. In addition, due to the excellent plasticity of unmelted TA2 and Q235, the residual stress of the joint can be reduced.

References

1. M. Gao, S.W. Mei, Z.M. Wang, X.Y. Li, X.Y. Zeng, Characterisation of laser welded dissimilar Ti/steel joint using Mg interlayer. Sci. Technol. Weld. Join **17**, 269–276 (2012)
2. C. Shuhai, Z. Mingxin, H. Jihua, Microstructures and mechanical property of laser butt welding of titanium alloy to stainless steel. Mater. Des. **53**, 504–511 (2014)
3. S. Kundu, M. Ghosh, A. Laik, K. Bhanumuthy, G.B. Kale, S. Chatterjee, Diffusion bonding of commercially pure titanium to 304 stainless steel using copper interlayer. Mater. Sci. Eng., A **407**, 154–160 (2005)

4. L. Wei, Y. Lei, K. Sreekar, L. Frank, N. Joseph, M. Karen, T. Brown, W.J. Seufzer, Ti–Fe intermetallics analysis and control in joining titanium alloy and stainless steel by Laser Metal Deposition. J. Mater. Process Technol. **242**, 39–48 (2017)

5. K. Ishida, Y. Gao, K. Nagatsuka, M. Takahashi, K. Nakata, Microstructures and mechanical properties of friction stir welded lap joints of commercially pure titanium and 304 stainless steel. J. Alloys Compd. **630**, 172–177 (2015)

6. S. Kundu, S. Chatterjee, Characterization of diffusion bonded joint between titanium and 304 stainless steel using a Ni interlayer. Mater. Charact. **59**, 631–637 (2008)

7. M. Ghosh, S. Chatterjee, Effect of interface microstructure on the bond strength of the diffusion welded joints between titanium and stainless steel. Mater. Charact. **54**, 327–337 (2005)

8. M. Lee, J. Park, J. Lee, C. Rhee, Phase-dependent corrosion of titanium-to-stainless steel joints brazed by Ag–Cu eutectic alloy filler and Ag interlayer. J. Nucl. Mater. **439**, 168–173 (2013)

9. Y. Zhang, D.Q. Sun, X.Y. Gu, Y.J. Liu, Nd/YAG pulsed laser welding of TC4 titanium alloy to 301L stainless steel via pure copper interlayer. Int. J. Adv. Manuf. Technol. **90**, 953–961 (2017)

10. E. Atasoy, N. Kahraman, Diffusion bonding of commercially pure titanium to low carbon steel using a silver interlayer. Mater. Charact. **59**, 1481–1490 (2008)

11. P. He, H. Yue, J.H. Zhan, Hot pressing diffusion bonding of a titanium alloy to a stainless steel with an aluminum alloy interlayer. Mater. Sci. Eng., A **486**, 171–176 (2008)

12. M. Gao, S.W. Mei, Characterisation of laser welded dissimilar Ti/steel joint using Mg interlayer. Sci. Technol. Weld. Join. **17**, 269–276 (2002)

13. Y. Zhang, D.Q. Sun, X.Y. Gu, L. HongMei, A hybrid joint based on two kinds of bonding mechanisms for Titanium alloy and stainless steel by pulsed laser welding. Mater. Lett. **185**, 152–155 (2016)

14. J.P. Oliveira, B. Panton, Z. Zeng, Laser joining of NiTi to Ti6Al4V using a niobium interlayer. Acta Mater. **105**, 9–15 (2016)

15. S. Kundu, S. Sam, S. Chatterjee, Evaluation of interface microstructure and mechanical properties of the diffusion bonded joints of Ti–6Al–4V alloy to micro-duplex stainless steel. Mater. Sci. Eng., A **528**, 4910–4916 (2011)

16. M. Fazel-Najafabadi, S.F. Kashani-Bozorg, Joining of CP-Ti to 304 stainless steel using friction stir welding technique. Mater. Des. **31**, 4800–4807 (2010)

17. S.A. Mousavi, P.F. Sartangi, Experimental investigation of explosive welding of Cp-titanium/AISI 304 Stainless steel. Mater. Des. **30**, 459–468 (2009)

18. W. Chen, A. Paul, M. Pal, CO_2 laser welding of galvanized steel sheets using vent holes. Mater. Des. **30**, 245–251 (2009)

19. K. Amit, Y. Duck, C. Darek, Correlation analysis of the variation of weld seam and tensile strength in laser welding of galvanized steel. Opt. Laser Eng. **51**, 1143–1152 (2013)

20. W.F. Ho, C.P. Jo, J.H.C. Lin, Structure and properties of cast binary Ti–Mo alloy. Biomaterials **20**, 2115–2122 (1999)

21. N.T.C. Oliveira, G. Aleixo, R. Caram, A.C. Guastaldi, Development of Ti–Mo alloys for biomedical applications: microstructure and electrochemical characterization. Mater. Sci. Eng., A **452–453**, 727–731 (2007)

22. G. Lüering, J.C. Willians, *Engineering Materials and Process: Titanium* (Springer, Heideberg, 2003)

23. W. Tian. *Experimental study on the laser welding of magnesium and aluminum dissimilar metal*. Master thesis, Hunan University, 2013

24. Ma. Xuyi, G. Shuili, L. Zhang Jiuxing, Y.J. Wei, Formation, microstructure and mechanical properties of double-sided laser beam welded Ti–6Al–4V T-joint. Trans. Nonferrous Metals Soc. China **26**, 729–735 (2016)

25. J.L. Murray, The Fe–Ti (iron–titanium) system. Bull. Alloy Phase Diagr. **2**, 320–334 (1981)

26. C. Yu, M.F. Wu, H. Lu, Factors influencing formation and growth of coarse Ti–Fe compound in Ti–Fe eutectic reaction. Sci. Technol. Weld. Join. **11**, 265–270 (2006)

27. S.A.A. Akbari Mousavi, P.F. Sartangi, Effect of post-weld heat treatment on the interface microstructure of explosively welded titanium-stainless steel composite. Mater. Sci. Eng. A **2008**(494), 329–336 (2008)

28. G.B. Kale, R.V. Patil, P.S. Gawade, Interdiffusion studies in titanium-304 stainless steel system. J. Nucl. Mater. **257**, 44–50 (1998)

29. B. Aleman, I. Gutierrez, J.J. Urcola, Interface microstructures in diffusion bonding of titanium alloys to stainless steel and low alloy steels. Mater. Sci. Technol. **9**, 633–641 (1993)

30. J. Song, A. Kostka, M. Veehmayer, D. Raabe, Hierarchical microstructure of explosive joints: example of titanium to steel cladding. Mater. Sci. Eng., A **528**, 2641–2647 (2011)

31. O. Torun, A. Karabulut, B. Baksan, I. Çelikyürek, Diffusion bonding of AZ91 using a silver interlayer. Mater. Des. **29**, 2043–2046 (2008)

32. Y.B. Chen, Z.L. Lei, L.Q. Li, L. Wu, Experimental study on welding characteristics of CO_2 laser TIG hybrid welding process. Sci. Technol. Weld. Join. **11**, 403–411 (2006)

33. T.P. Isaac, M. Dollar, T.B. Massalaki, Metall. Trans. A **19A**, 675–686 (1988)

34. D. Ye, J. Hu, *Thermodynamic Data Manual of Practical Inorganic Materials* (Metallurgical Industry Press, Beijing, 2002)

35. Y.C. Hong, W. Zhang, Relationship between overlap rate of weld spots and solidification characteristic for pulsed laser welding. Heat Treat. **4**, 13–19 (2014)